

# Crystal structure of a translation termination complex formed with release factor RF2

Andrei Korostelev<sup>a,b,1</sup>, Haruichi Asahara<sup>a,b,1,2</sup>, Laura Lancaster<sup>a,b,1</sup>, Martin Laurberg<sup>a,b</sup>, Alexander Hirschi<sup>a,b</sup>, Jianyu Zhu<sup>a,b</sup>, Sergei Trakhanov<sup>a,b</sup>, William G. Scott<sup>a,c</sup>, and Harry F. Noller<sup>a,b,3</sup>

<sup>a</sup>Center for Molecular Biology of RNA and Departments of <sup>b</sup>Molecular, Cell and Developmental Biology and <sup>c</sup>Chemistry and Biochemistry, University of California, Santa Cruz, CA 95064

Contributed by Harry F. Noller, October 30, 2008 (sent for review October 22, 2008)

**We report the crystal structure of a translation termination complex formed by the *Thermus thermophilus* 70S ribosome bound with release factor RF2, in response to a UAA stop codon, solved at 3 Å resolution. The backbone of helix  $\alpha 5$  and the side chain of serine of the conserved SPF motif of RF2 recognize U1 and A2 of the stop codon, respectively. A3 is unstacked from the first 2 bases, contacting Thr-216 and Val-203 of RF2 and stacking on G530 of 16S rRNA. The structure of the RF2 complex supports our previous proposal that conformational changes in the ribosome in response to recognition of the stop codon stabilize rearrangement of the switch loop of the release factor, resulting in docking of the universally conserved GGQ motif in the PTC of the 50S subunit. As seen for the RF1 complex, the main-chain amide nitrogen of glutamine in the GGQ motif is positioned to contribute directly to catalysis of peptidyl-tRNA hydrolysis, consistent with mutational studies, which show that most side-chain substitutions of the conserved glutamine have little effect. We show that when the H-bonding capability of the main-chain N-H of the conserved glutamine is eliminated by substitution with proline, peptidyl-tRNA esterase activity is abolished, consistent with its proposed role in catalysis.**

70S ribosome structure | stop codon recognition | polypeptide release

In bacteria, termination of protein synthesis depends on the type I release factors, RF1 and RF2, which are required for recognition of the stop codons and for hydrolysis of the peptidyl-tRNA ester bond. Our understanding of the mechanism of termination faces three main questions: (i) How are stop codons recognized? Unlike the sense codons, there are no corresponding cognate tRNAs to recognize nonsense codons. Are they recognized directly by the release factors, or indirectly, for example through ribosomal RNA? (ii) What is the mechanism of peptidyl-tRNA hydrolysis? Is the esterase reaction catalyzed directly by the release factors, or by the ribosome? And (iii) How is peptidyl-tRNA hydrolysis coupled to stop codon recognition?

Termination at the UAG stop codon depends on RF1, UGA on RF2, and UAA on either of the two factors (1–3). Thus, although the two release factors have similar overall structures (4–6) and both recognize codons of the general type URR, RF1 is able to discriminate between A and G at the second position whereas RF2 discriminates between A and G at the third position. Determinants for codon specificity were localized to domain 2 of the release factors, in particular to the conserved PxT and SPF motifs of RF1 and RF2, respectively, based on genetic studies in which swapping these motifs was found to switch codon specificity (7, 8). A “tripeptide anticodon” mechanism for stop-codon recognition was proposed, in which the PxT and SPF motifs recognize the corresponding stop codons (7, 8). In a recent 3.2 Å crystal structure of a termination complex containing RF1, Thr-186 of the PxT motif was indeed found to be a critical recognition element of RF1, interacting directly with the UA dinucleotide in the first and second positions of the UAA stop codon (9). The third-position A was seen to be unstacked from the rest of the codon, sandwiched between Ile-192 of RF1

and G530 of 16S rRNA, and recognized separately by interactions with Gln-181 and Thr-194. Stop codon recognition by RF1 also involves a network of interactions with other structural elements of RF1, including critical main-chain atoms and conserved features of 16S rRNA (9).

Many studies have implicated the conserved GGQ motif in domain 3, present in the release factors of all three primary domains of life, in the hydrolysis reaction. Although the side chain of the conserved glutamine has been proposed to play a role in catalysis (10, 11), elimination of its side-chain amide group by mutation of this residue to alanine, for example, confers only a small decrease in catalytic activity (12–14). This was rationalized by the structure of the RF1 termination complex, which showed that the side chain of the glutamine is directed away from the scissile bond, whereas its main-chain amide is positioned to participate in catalysis through product and/or transition-state stabilization (9). This unexpected result also explains why substitutions of the neighboring glycine cause severe defects in peptide release (14–16): introduction of a side chain would block access of the main-chain amide of the glutamine to the reaction center.

The structure of the RF1 complex also suggested a mechanism for how codon recognition is coupled to peptidyl-tRNA hydrolysis. Upon recognition of the UAA stop codon, G530 and A1492 flip out, but A1493, which would clash with domain 2 of RF1 if flipped as in sense codon recognition (17), remains stacked within helix 44; A1913 of 23S rRNA then stacks on A1493 of 16S rRNA. The interface between the rearranged decoding site and the reading head of the factor thus forms a binding site for an altered conformation of the “switch” loop, which links domains 3 and 4 of RF2 (Fig. 1), forming a rigid connector that places domain 3 and its GGQ motif in contact with the peptidyl-tRNA ester linkage in the peptidyl transferase center of the 50S subunit. This scenario is consistent with the observations that deletion of helix 69 of 23S rRNA, whose apical loop contains A1913, results in a specific defect in RF1-dependent peptidyl-tRNA hydrolysis (18), and that paromomycin, which induces flipping out of both A1492 and A1493 (17), and which occupies the site vacated by the flipped A1493, inhibits termination, but not sense codon recognition (19).

Here, we report the crystal structure of a translation termination complex containing release factor RF2 bound in response

Author contributions: A.K., H.A., L.L., W.G.S., and H.F.N. designed research; A.K., H.A., L.L., M.L., A.H., J.Z., and S.T. performed research; and A.K., M.L., and H.F.N. wrote the paper.

The authors declare no conflict of interest.

Data deposition: The atomic coordinates and structure factors have been deposited with the Protein Data Bank, [www.pdb.org](http://www.pdb.org) (PDB ID codes 3F1E, 3F1F, 3F1G, and 3F1H).

<sup>1</sup>A.K., H.A., and L.L. contributed equally to this work.

<sup>2</sup>Present address: New England Biolabs, Ipswich, MA 01938.

<sup>3</sup>To whom correspondence should be addressed. E-mail: [harry@nuvolari.ucsc.edu](mailto:harry@nuvolari.ucsc.edu).

This article contains supporting information online at [www.pnas.org/cgi/content/full/0810953105/DCSupplemental](http://www.pnas.org/cgi/content/full/0810953105/DCSupplemental).

© 2008 by The National Academy of Sciences of the USA

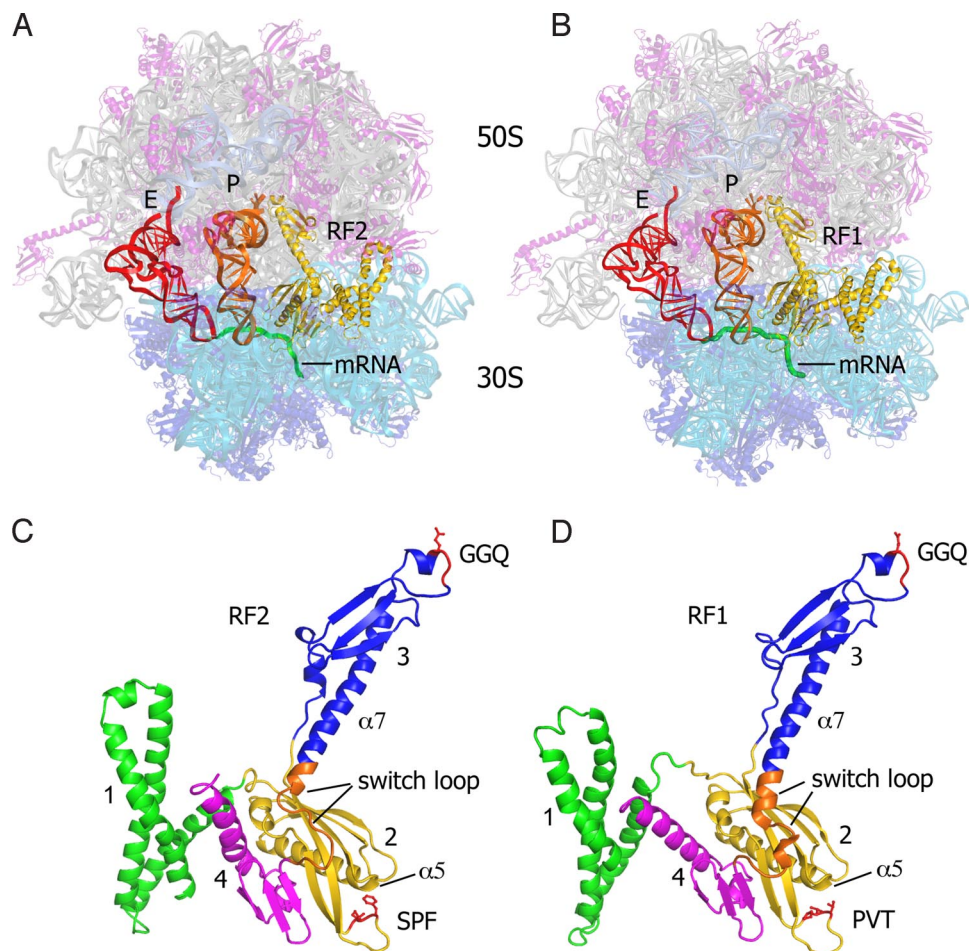


**Fig. 1.** Comparison of the structures of the RF1 and RF2 termination complexes. (A) RF2 termination complex (this work), showing RF2 (yellow), P-site tRNA (orange), E-site tRNA (red), mRNA (green), 16S rRNA (cyan), 23S and 5S rRNA (gray), 30S proteins (blue), and 50S proteins (magenta). (B) RF1 termination complex (9); molecular components are colored similarly as in A. (C) RF2 in its ribosome-bound conformation, rotated  $\approx 180^\circ$  from the view shown in A, with domains numbered. The GGQ and SPF motifs are shown in red, and the switch loop is shown in orange. (D) RF1 in its ribosome-bound conformation. The GGQ and PVT motifs are indicated in red and the switch loop is shown in orange.

to a UAA codon, solved at  $3\text{\AA}$  resolution. The different codon recognition specificities of RF1 and RF2 can be rationalized by structural differences in the decoding center, where Ser-206 of the SPF motif of RF2 interacts directly with the second base and Thr-216 recognizes A3 of the stop codon. Despite considerable sequence divergence in the sequences of the switch loops of RF1 and RF2, the switch loop of RF2 also undergoes a conformational change that is likely involved in coupling codon recognition to the positioning of domain 3 (4). The GGQ motif of RF2 is positioned essentially identically to that seen for the RF1 complex, again implicating the main-chain amide nitrogen of the conserved glutamine in catalysis of peptidyl-tRNA hydrolysis. Finally, when the H-bonding capability of the main-chain N-H of the Gln is eliminated by substitution with proline, activity is abolished, consistent with its proposed role in catalysis.

## Results and Discussion

**Interaction with the L11 Stalk.** The overall position and conformation of RF2 in the 70S ribosome are similar to those of RF1 (5, 9, 20, 21). The main difference between the two structures is found in the positioning of domain 1 of the factor. In the X-ray structures of the RF1 complex, no contact was observed between domain 1 and the L11 stalk of the 50S subunit (5, 9). By contrast, in the RF2 complex, the distal end of domain 1 is  $12\text{\AA}$  closer to the ribosomal A site, placing it in contact with the L11 stalk (Fig.

S1), in agreement with low-resolution X-ray studies of the RF2 complex (5). Interactions with 23S rRNA occur at the loops of helices 43 (at A1067) and 44 (at A1095), where the conserved Trp-52 stacks on A1095 (Fig. S1B). The sole protein-protein contacts involve packing of helix  $\alpha 1$  of RF2 against the proline-rich helix  $\alpha 1$  near the N terminus of L11 (Fig. S1B). The possible biological significance of this difference between the RF1 and RF2 termination complexes is unclear.

**Stop Codon Recognition.** In previous studies, the universally conserved nucleotides A530, A1492 and A1493 of 16S ribosomal RNA in the decoding center of the 30S subunit were found to undergo striking rearrangements in response to recognition of a sense codon by cognate tRNA (17, 22), binding of IF1 (23), binding of antibiotics (17, 24, 25) or recognition of a stop codon by RF1 (9). In the RF2 termination complex, G530 and A1492 flip out of their resting states, whereas A1493 remains stacked on the end of helix 44 and A1913 of 23S rRNA stacks on A1493, as observed for the RF1 complex (9) (Fig. 2A and Fig. S2). Also, unlike the conformation seen for sense codons, the third nucleotide of the stop codon (A3) is again found to be unstacked from the first 2 nt and is instead stacked on the flipped G530 of 16S rRNA. Thus, as for the RF1 complex, the first 2 bases of the stop codon are read separately from the third base by RF2.

Strong specificity for U in the first position (26) is determined





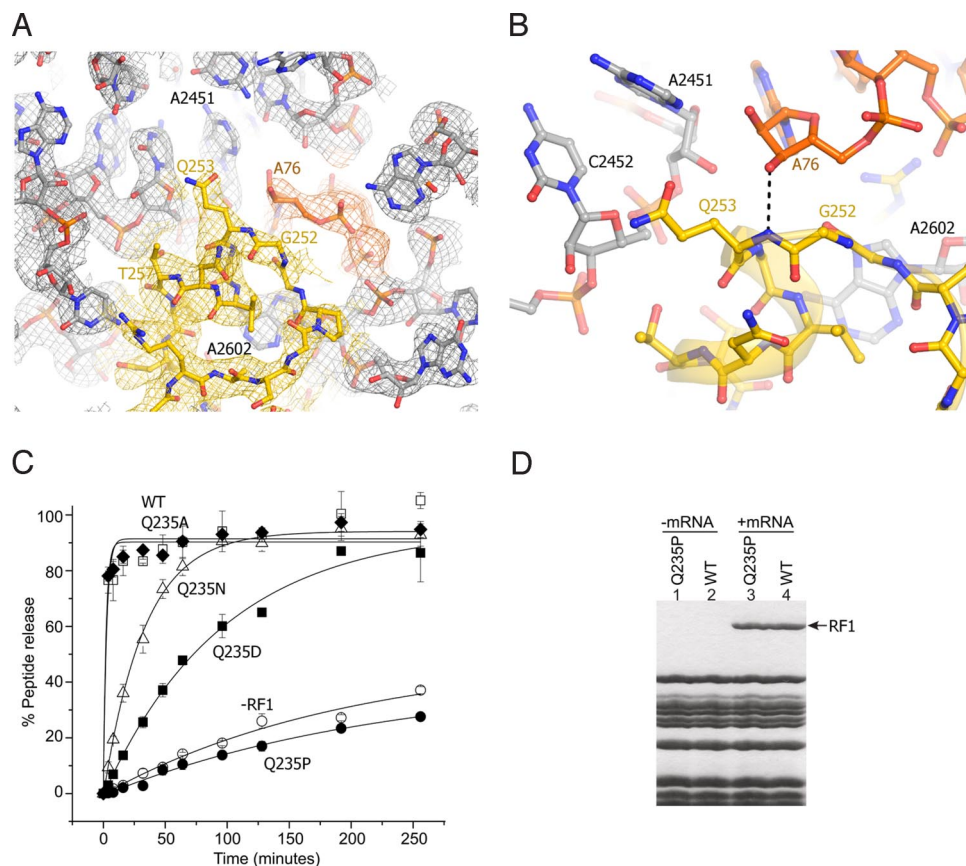


**Fig. 4.** Interactions of the GGQ region of RF2 at the site of catalysis. (A)  $\sigma_A$ -weighted  $3F_{\text{obs}} - 2F_{\text{calc}}$  electron density for RF2 (yellow), P-site tRNA (orange) and 23S rRNA (gray), contoured at  $1.7 \sigma$ . (B) Orientation of Gln-253 of the RF2 GGQ motif. The backbone amide nitrogen of Gln-253 is positioned to H-bond with the 3'-OH of A76 of P-site tRNA, whereas its side chain is oriented away from the reaction site. (C) The Q235P mutation abolishes peptide release activity of *E. coli* RF1. Model 70S termination complexes assembled with [ $^{35}\text{S}$ ]fMet-tRNA<sup>fMet</sup> in the P site and mRNA M0–27 (which contains an AUG codon followed a UAA stop codon), were incubated at 37 °C with (open squares) wild-type RF1, or the RF1 mutants (diamonds) Q235A (filled squares) Q235D (triangles) Q235N (filled circles) Q235P, or (open circles) no RF1. Peptide release was monitored by measuring the amount of [ $^{35}\text{S}$ ]fMet extracted into ethyl acetate at the indicated time points. Error bars indicate the range of values from 2 or 3 independent experiments, which were averaged and fit to single-exponential curves to determine the rates of peptide release. (D) Mutant Q235P RF1 binds normally in a stop-codon-dependent manner. Lanes 1 and 2, neither wild-type nor Q235P RF1 binds to ribosomes in the absence of mRNA. Lanes 3 and 4, in the presence of mRNA MO-27, both Q235P and wild-type RF1 bind stoichiometrically to ribosomes.

hydrolysis is observed (Fig. 4C and Table S1). Although catalytically inactive, GGP mutant RF1 retains stoichiometric, codon-dependent binding to ribosomes (Fig. 4D).

Although this result cannot be taken as definitive evidence for the participation of the Gln-235 (Gln-230 or Gln-253 in *T. th.* RF1 and RF2, respectively) backbone amide in catalysis, because of the possible influence of proline substitution on backbone conformation, it is consistent with our proposal. Deleterious effects of proline substitution have been interpreted as evidence for participation of the backbone amide group in catalysis by serine proteases (36) and GTPases (37). Moreover, concern that introduction of proline into an active site can indirectly affect catalysis is mitigated by high-resolution X-ray structures of a G119P mutant of thrombin (36) and of an A30P mutant of Rab5a (38), in which proline substitutions fail to cause significant conformational changes. In this regard, an *in silico* test of the effect of the Q253P mutation, in which we modeled the mutant factor, suggests that the proline substitution would be unlikely to induce significant changes in the conformations of RF1 or the surrounding features in the ribosomal PTC (Fig. S7). This can be explained by the similarities between the main-chain (39) torsion angles for Gln-230 in the experimental structure (9) to those typically observed for proline (Fig. S7) in high-resolution crystal structures (39). Beyond these circumstantial arguments, defini-

tive evidence will require determination of the structure of a termination complex containing the mutant factor.

## Materials and Methods

Procedures for crystallization and structure determination were similar to those described (9). The structure was determined by molecular replacement followed by refinement yielding  $R/R^{\text{free}}$  of 0.28/0.316 (Table S2). A detailed account of structure determination procedures is given in *SI Materials and Methods*.

The construction and isolation of mutant RF1 and peptide release assay was as follows: The RF1 gene from *E. coli* MRE600 was cloned into pET21b (Novagen) to obtain C-terminal 6His-tagged RF1. Mutations at position Q235 were generated by site-directed mutagenesis (40). RF1 proteins were expressed and purified on Ni-NTA agarose resin (Qiagen) using standard procedures, then additionally purified by FPLC chromatography on a 24-mL Superdex 75 gel filtration column (Amersham Pharmacia); proteins were stored in 50 mM Tris-HCl (pH 7.0), 60 mM  $\text{NH}_4\text{Cl}$ , 10 mM  $\text{MgCl}_2$ , and 5 mM  $\beta$ -mercaptoethanol ( $\beta$ ME) at  $-80^\circ\text{C}$ .

30S and 50S subunits were prepared from salt-washed MRE600 ribosomes as described (41, 42). tRNA<sup>fMet</sup> was aminoacylated as described in ref. 43. 30S subunits were heat-activated at 42 °C for 10 min in Buffer A [50 mM KHepes (pH 7.6), 75 mM  $\text{NH}_4\text{Cl}$ , 20 mM  $\text{MgCl}_2$ , 5 mM  $\beta$ ME] before use in each assay.

Model 70S ribosome termination complexes were formed by incubating 30S subunits (1  $\mu\text{M}$ ), 50S subunits (1.2  $\mu\text{M}$ ), M0–27 mRNA (2  $\mu\text{M}$ ), and [ $^{35}\text{S}$ ]fMet-tRNA<sup>fMet</sup> (0.5  $\mu\text{M}$ ) for 20 min at 37 °C in Buffer A. The [ $\text{Mg}^{2+}$ ] was reduced to 10 mM by addition of buffer A lacking  $\text{MgCl}_2$ . For peptide release assays, the complex was added to a 6-fold molar excess of RF1 and incubated

in Buffer A (10 mM MgCl<sub>2</sub>) at 37 °C. Aliquots were removed from the reaction at each time point and quenched in 5 vol of 0.1 M HCl; hydrolyzed [<sup>35</sup>S]fMet was extracted with 1 mL of ethyl acetate, 0.7 mL of which was added to scintillation mixture and counted.

For RF1 binding assays, the 70S complex was formed as above, but with 2 μM [<sup>35</sup>S]fMet-tRNA<sup>fMet</sup>, and with or without M0–27 mRNA. As above, each complex was added to a 6-fold excess of RF1, then incubated at 37 °C for 5 min in Buffer A (10 mM MgCl<sub>2</sub>). Reactions were passed through a Sephacryl S200-HR resin (Sigma) 1-mL spin column, then precipitated with 4 vol of

acetone (–20 °C for 1 h), dissolved in loading buffer, and electrophoresed on a 12% acrylamide SDS gel.

**ACKNOWLEDGMENTS.** We thank John Paul Donohue for assistance with data processing and computational support; Eric Maklan for helpful discussions regarding kinetic measurements; and the beamline staffs at SSRL, ALS, and APS for their expert support during screening and data collection. These studies were supported by grants from the National Institutes of Health and the National Science Foundation (to H.F.N.) and a fellowship from the Danish Research Council (to M.L.).

1. Capecchi MR, Klein HA (1969) Characterization of three proteins involved in polypeptide chain termination. *Cold Spring Harbor Symp Quant Biol* 34:469–477.
2. Scolnick E, Tompkins R, Caskey T, Nirenberg M (1968) Release factors differing in specificity for terminator codons. *Proc Natl Acad Sci USA* 61:768–774.
3. Scolnick EM, Caskey CT (1969) Peptide chain termination. V. The role of release factors in mRNA terminator codon recognition. *Proc Natl Acad Sci USA* 64:1235–1241.
4. Vestergaard B, et al. (2001) Bacterial polypeptide release factor RF2 is structurally distinct from eukaryotic eRF1. *Mol Cell* 8:1375–1382.
5. Petry S, et al. (2005) Crystal structures of the ribosome in complex with release factors RF1 and RF2 bound to a cognate stop codon. *Cell* 123:1255–1266.
6. Shin DH, et al. (2004) Structural analyses of peptide release factor 1 from *Thermotoga maritima* reveal domain flexibility required for its interaction with the ribosome. *J Mol Biol* 341:227–239.
7. Ito K, Uno M, Nakamura Y (2000) A tripeptide “anticodon” deciphers stop codons in messenger RNA. *Nature* 403:680–684.
8. Nakamura Y, Ito K (2002) A tripeptide discriminator for stop codon recognition. *FEBS Lett* 514:30–33.
9. Laurberg M, et al. (2008) Structural basis for translation termination on the 70S ribosome. *Nature* 454:852–857.
10. Song H, et al. (2000) The crystal structure of human eukaryotic release factor eRF1—mechanism of stop codon recognition and peptidyl-tRNA hydrolysis. *Cell* 100:311–321.
11. Trobro S, Aqvist J (2007) A model for how ribosomal release factors induce peptidyl-tRNA cleavage in termination of protein synthesis. *Mol Cell* 27:758–766.
12. Seit Nebi A, Frolova L, Ivanova N, Poltarau A, Kiselev L (2000) Mutation of a glutamine residue in the universal tripeptide GGQ in human eRF1 termination factor does not cause complete loss of its activity. *Mol Biol (Moscow)* 34:899–900.
13. Seit-Nebi A, Frolova L, Justesen J, Kiselev L (2001) Class-1 translation termination factors: Invariant GGQ minidomain is essential for release activity and ribosome binding but not for stop codon recognition. *Nucleic Acids Res* 29:3982–3987.
14. Shaw JJ, Green R (2007) Two distinct components of release factor function uncovered by nucleophile partitioning analysis. *Mol Cell* 28:458–467.
15. Frolova LY, et al. (1999) Mutations in the highly conserved GGQ motif of class 1 polypeptide release factors abolish ability of human eRF1 to trigger peptidyl-tRNA hydrolysis. *Rna* 5:1014–1020.
16. Zavalov AV, Mora L, Buckingham RH, Ehrenberg M (2002) Release of peptide promoted by the GGQ motif of class 1 release factors regulates the GTPase activity of RF3. *Mol Cell* 10:789–798.
17. Ogle JM, et al. (2001) Recognition of cognate transfer RNA by the 30S ribosomal subunit. *Science* 292:897–902.
18. Ali IK, Lancaster L, Feinberg J, Joseph S, Noller HF (2006) Deletion of a conserved, central ribosomal intersubunit RNA bridge. *Mol Cell* 23:865–874.
19. Youngman EM, He SL, Nikstad LJ, Green R (2007) Stop codon recognition by release factors induces structural rearrangement of the ribosomal decoding center that is productive for peptide release. *Mol Cell* 28:533–543.
20. Rawat UB, et al. (2003) A cryo-electron microscopic study of ribosome-bound termination factor RF2. *Nature* 421:87–90.
21. Rawat U, et al. (2006) Interactions of the release factor RF1 with the ribosome as revealed by cryo-EM. *J Mol Biol* 357:1144–1153.
22. Selmer M, et al. (2006) Structure of the 70S ribosome complexed with mRNA and tRNA. *Science* 313:1935–1942.
23. Carter AP, et al. (2001) Crystal structure of an initiation factor bound to the 30S ribosomal subunit. *Science* 291:498–501.
24. Borovinskaya MA, et al. (2007) Structural basis for aminoglycoside inhibition of bacterial ribosome recycling. *Nat Struct Mol Biol* 14:727–732.
25. Francois B, et al. (2005) Crystal structures of complexes between aminoglycosides and decoding A site oligonucleotides: Role of the number of rings and positive charges in the specific binding leading to miscoding. *Nucleic Acids Res* 33:5677–5690.
26. Freistrotter DV, Kwiatkowski M, Buckingham RH, Ehrenberg M (2000) The accuracy of codon recognition by polypeptide release factors. *Proc Natl Acad Sci USA* 97:2046–2051.
27. Basu G, Sivanesan D, Kawabata T, Go N (2004) Electrostatic potential of nucleotide-free protein is sufficient for discrimination between adenine and guanine-specific binding sites. *J Mol Biol* 342:1053–1066.
28. Sponer J, Leszczynski J, Hobza P (1996) Structures and energies of hydrogen-bonded DNA base pairs. A nonempirical study with inclusion of electron correlation. *J Phys Chem* 100:1965–1974.
29. Tate WP, et al. (1995) Translational termination efficiency in both bacteria and mammals is regulated by the base following the stop codon. *Biochem Cell Biol* 73:1095–1103.
30. Poole ES, Major LL, Mannering SA, Tate WP (1998) Translational termination in *Escherichia coli*: Three bases following the stop codon cross-link to release factor 2 and affect the decoding efficiency of UGA-containing signals. *Nucleic Acids Res* 26:954–960.
31. Amort M, et al. (2007) An intact ribose moiety at A2602 of 23S rRNA is key to trigger peptidyl-tRNA hydrolysis during translation termination. *Nucleic Acids Res* 35:5130–5140.
32. Polacek N, et al. (2003) The critical role of the universally conserved A2602 of 23S ribosomal RNA in the release of the nascent peptide during translation termination. *Mol Cell* 11:103–112.
33. Youngman EM, Brunelle JL, Kochaniak AB, Green R (2004) The active site of the ribosome is composed of two layers of conserved nucleotides with distinct roles in peptide bond formation and peptide release. *Cell* 117:589–599.
34. Wilmouth RC, et al. (2001) X-ray snapshots of serine protease catalysis reveal a tetrahedral intermediate. *Nat Struct Biol* 8:689–694.
35. Jaeger KE, Dijkstra BW, Reetz MT (1999) Bacterial biocatalysts: Molecular biology, three-dimensional structures, and biotechnological applications of lipases. *Annu Rev Microbiol* 53:315–351.
36. Bobofchak KM, Pineda AO, Mathews FS, Di Cera E (2005) Energetic and structural consequences of perturbing Gly-193 in the oxyanion hole of serine proteases. *J Biol Chem* 280:25644–25650.
37. Liang Z, Mather T, Li G (2000) GTPase mechanism and function: New insights from systematic mutational analysis of the phosphate-binding loop residue Ala30 of Rab5. *Biochem J* 346 (Pt 2):501–508.
38. Zhu G, et al. (2003) High resolution crystal structures of human Rab5a and five mutants with substitutions in the catalytically important phosphate-binding loop. *J Biol Chem* 278:2452–2460.
39. Ramachandran GN, Ramakrishnan C, Sasisekharan V (1963) Stereochemistry of polypeptide chain configurations. *J Mol Biol* 7:95–99.
40. Kunkel TA (1985) Rapid and efficient site-specific mutagenesis without phenotypic selection. *Proc Natl Acad Sci USA* 82:488–492.
41. Moazed D, Noller HF (1989) Interaction of tRNA with 23S rRNA in the ribosomal A, P, and E sites. *Cell* 57:585–597.
42. Moazed D, Noller HF (1986) Transfer RNA shields specific nucleotides in 16S ribosomal RNA from attack by chemical probes. *Cell* 47:985–994.
43. Lancaster L, Noller HF (2005) Involvement of 16S rRNA nucleotides G1338 and A1339 in discrimination of initiator tRNA. *Mol Cell* 20:623–632.

# Supporting Information

Korostelev *et al.* 10.1073/pnas.0810953105

## SI Materials and Methods

**Crystallization.** Ribosomes were purified from *Thermus thermophilus* as described (1) with the following modifications. After column chromatography on Toyo-Pearl Butyl 650S, the buffer of the eluted ribosome fraction was replaced with buffer E (25 mM Tris-OAc, pH 7.0, 50 mM KOAc, 10 mM NH<sub>4</sub>OAc, 10 mM Mg(OAc)<sub>2</sub>), using Centricon Plus YM-100 (Amicon). An equal volume of microcrystallization solution (100 mM Tris-OAc, pH 7.0, 200 mM KSCN, 7% PEG20k, 15% PEG200, 2.8% deoxy-BigChap) was then added at room temperature, and the mixture was stored at 4 °C. After a few days, microcrystals were harvested and dissolved in buffer E. The ribosome concentration was adjusted to 20 mg/ml, and stored in aliquots at -80 °C until used for complex formation.

The mRNA M0-27 [GGC AAG GAG GUA AAA AUG UAA AAA AAA] was chemically synthesized (IDT) (1). *Escherichia coli* tRNA<sup>fMet</sup> was purchased from Sigma-Aldrich. The gene for *T. thermophilus* RF2 lacking T52 from the start codon where a frameshift occurs was cloned into pET24b. RF2 was purified using the same procedure reported for RF1 (1). The 70S:mRNA:tRNA<sup>fMet</sup>:RF2 termination complex was formed as described for the RF1 complex (1), using the molar ratios 1:2:2.4:4, respectively. Crystallization and cryoprotection procedures were as described (1).

**x-ray data collection and structure determination.** Crystals were screened at beamlines 7.1, 9.1, 9.2 and 11.1 at the Stanford Synchrotron Radiation Laboratory, and at beamline 4.2.2 at the

Advanced Light Source, Lawrence Berkeley National Laboratory. x-ray diffraction data were recorded at beamline 23 ID-D at the Advanced Photon Source at Argonne National Laboratory using an x-ray wavelength of 0.9537 Å and an oscillation angle of 0.2°. Data from four datasets obtained from different positions of the same crystal were integrated and merged using the XDS package (2), scaled in SCALA (3) and truncated in TRUNCATE (4). 1% of reflections were marked as test-set ( $R^{\text{free}}$  set) reflections to monitor the progress of refinement.

Structure determination started with rigid-body refinement of the previously determined structure of the RF1 termination complex, which was obtained from the same crystal form (1). At this stage of refinement, release factor was not included in the structure. Secondary structure elements and some side chains of RF2 were visible in the starting Fourier difference maps (Fig. S3). The 1.8 Å structure of free *E. coli* RF2 (5) was modified to fit the difference map obtained after rigid-body refinement. The sequence was modified to that of *T. thermophilus* RF2 employing T-COFFEE (6) and MODELLER (7). The 2.5 Å structure of free *T. thermophilus* RF2 (8) was used as an aid in modeling several flexible parts of the release factor. After simulated annealing and B-factor refinement in CNS (9), the structure of the RF2 termination complex was subjected to TLS refinement in PHENIX (10), yielding good stereochemistry and crystallographic statistics (Table S2). NCS restraints were used throughout the refinement as described (1). PYMOL (11), O (12) and local real-space refinement (13) were used for model building. Figs. were rendered using PYMOL (11).

1. Laurberg M, *et al.* (2008) Structural basis for translation termination on the 70S ribosome. *Nature* 454:852–857.
2. Kabsch W (1993) Automatic processing of rotation diffraction data from crystals of initially unknown symmetry and cell constants. *J Appl Crystallogr* 26:795–800.
3. Evans P (2006) Scaling and assessment of data quality. *Acta Crystallogr D* 62:72–82.
4. CCP4 (1994) The CCP4 suite: Programs for protein crystallography. *Acta Crystallogr D Biol Crystallogr* 50:760–763.
5. Vestergaard B, *et al.* (2001) Bacterial polypeptide release factor RF2 is structurally distinct from eukaryotic eRF1. *Mol Cell* 8:1375–1382.
6. Notredame C, Higgins DG, Heringa J (2000) T-Coffee: A novel method for fast and accurate multiple sequence alignment. *J Mol Biol* 302:205–217.
7. Eswar N, *et al.* (2007) Comparative protein structure modeling using MODELLER. *Curr Protocols Protein Sci* Chapter 2, Unit 29.
8. Zoldak G, *et al.* (2007) Release factors 2 from *Escherichia coli* and *Thermus thermophilus*: structural, spectroscopic and microcalorimetric studies. *Nucleic Acids Res* 35:1343–1353.
9. Brunger AT, *et al.* (1998) Crystallography & NMR system: A new software suite for macromolecular structure determination. *Acta Crystallogr D* 54:905–921.
10. Adams PD, *et al.* (2002) PHENIX: Building new software for automated crystallographic structure determination. *Acta Crystallogr D* 58:1948–1954.
11. DeLano WL (2002) The PyMOL Molecular Graphics System (Delano Scientific, Palo Alto, CA).
12. Jones TA., Zou JY, Cowan SW, Kjeldgaard M (1991) Improved methods for building protein models in electron density maps and the location of errors in these models. *Acta Crystallogr A* 47 (Pt 2):110–119.
13. Korostelev A, Bertram R, Chapman MS (2002) Simulated-annealing real-space refinement as a tool in model building. *Acta Crystallogr D* 58:761–767.





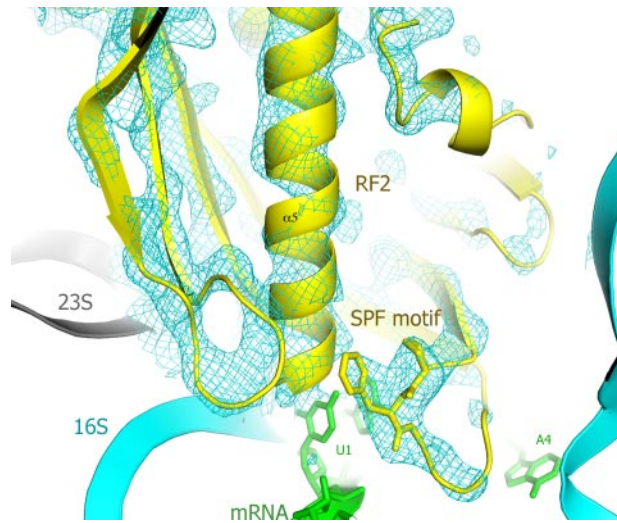


**Fig. S3.** Unbiased  $\sigma_A$ -weighted  $3F_{\text{obs}}-2F_{\text{calc}}$  electron density map calculated before inclusion of RF2 into the model. Proline and phenylalanine side chains of the fully conserved SPF motif implicated in recognition of the stop codon can be unambiguously identified in this initial map (cyan). The final refined model for RF2 (yellow), mRNA (green), 16S (cyan) and 23S (gray) rRNA is shown.

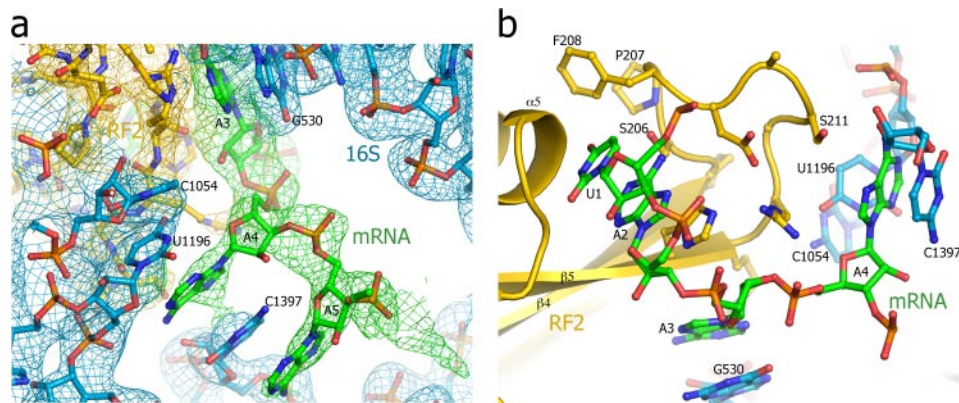


**Fig. S4.** Interactions of the stop codon and downstream nucleotides (A4 and A5) of mRNA with the ribosome. (a)  $\sigma_A$ -weighted  $3F_{\text{obs}} - 2F_{\text{calc}}$  electron density map showing intercalation of A4 between U1196 and C1397 of 16S rRNA (cyan), while C1397 in turn is intercalated between A4 and A5 of mRNA (green). Densities attributed to 16S rRNA and RF2 are contoured at  $1\sigma$ ; mRNA at  $0.8\sigma$ . (b) The network of stacking interactions in the decoding center involving stop codon nucleotides and A4.

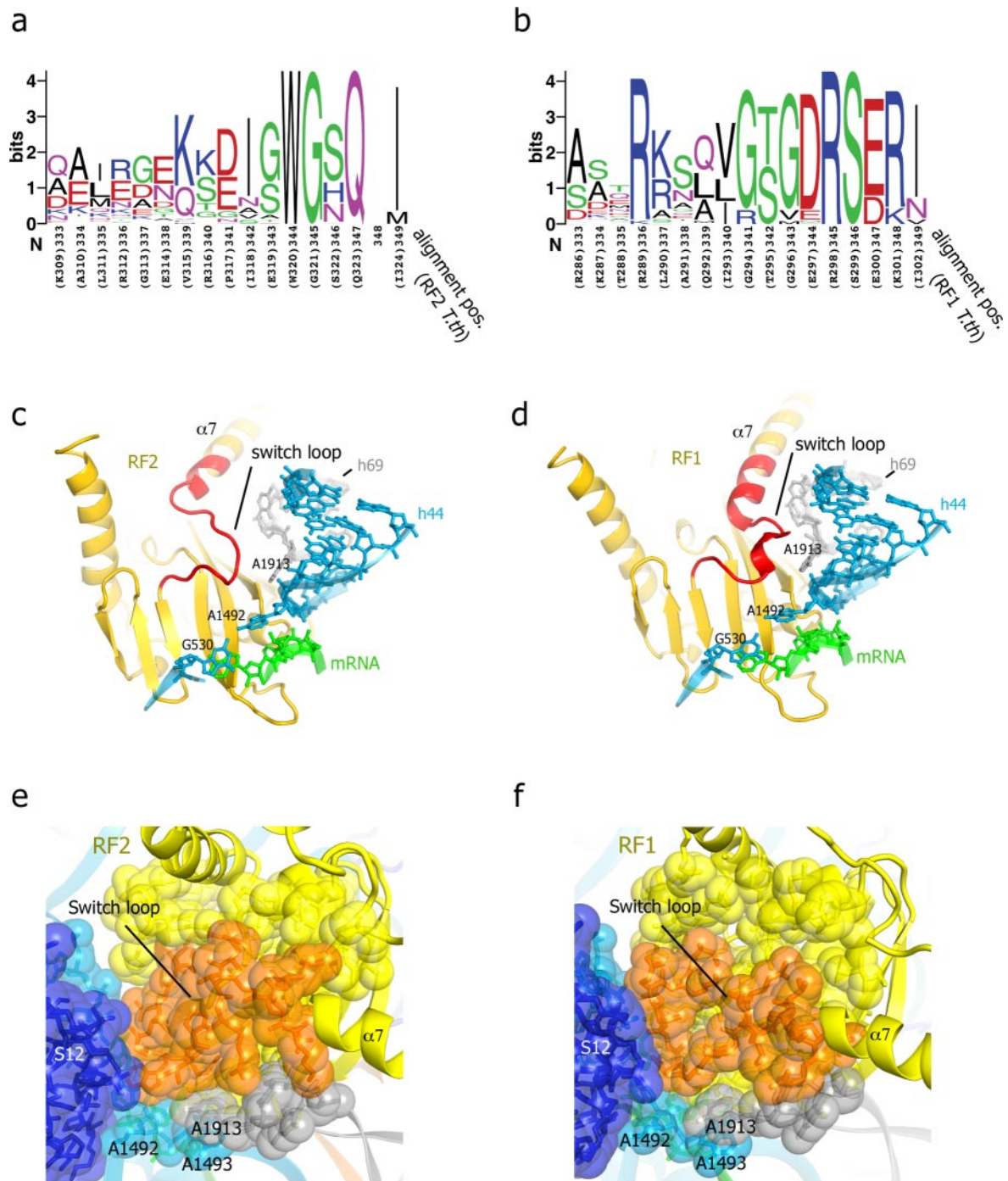


**Fig. S5.** Sequence divergence and similarity of packing of the switch loops of RF2 (this work) and RF1 (1) at the decoding center of the ribosome. (a) Comparison of switch loop sequences between 62 sequences of prokaryotic RF2. (b) Comparison of switch loop sequences between 63 sequences of prokaryotic RF1. Positions for alignment between the RF1 and RF2 sequences, and in parentheses, the sequences of *T.th* RF2 and *T.th* RF1, respectively, are given in a and b. Sequence alignments were performed in T-COFFEE (6) and sequence logos generated in SEQLOGO [Crooks GE, Hon G, Chandonia JM, Brenner SE (2004) WebLogo: a sequence logo generator. *Genome Res* 14:1188–1190]. (c and d) The switch loop of RF2 or RF1 extends helix  $\alpha 7$  and packs at the interface of protein S12, A1913 of 23S rRNA and A1492 of 16S rRNA. (e and f) Packing of the switch loop against the decoding center in the RF2 and RF1-bound complexes, respectively.

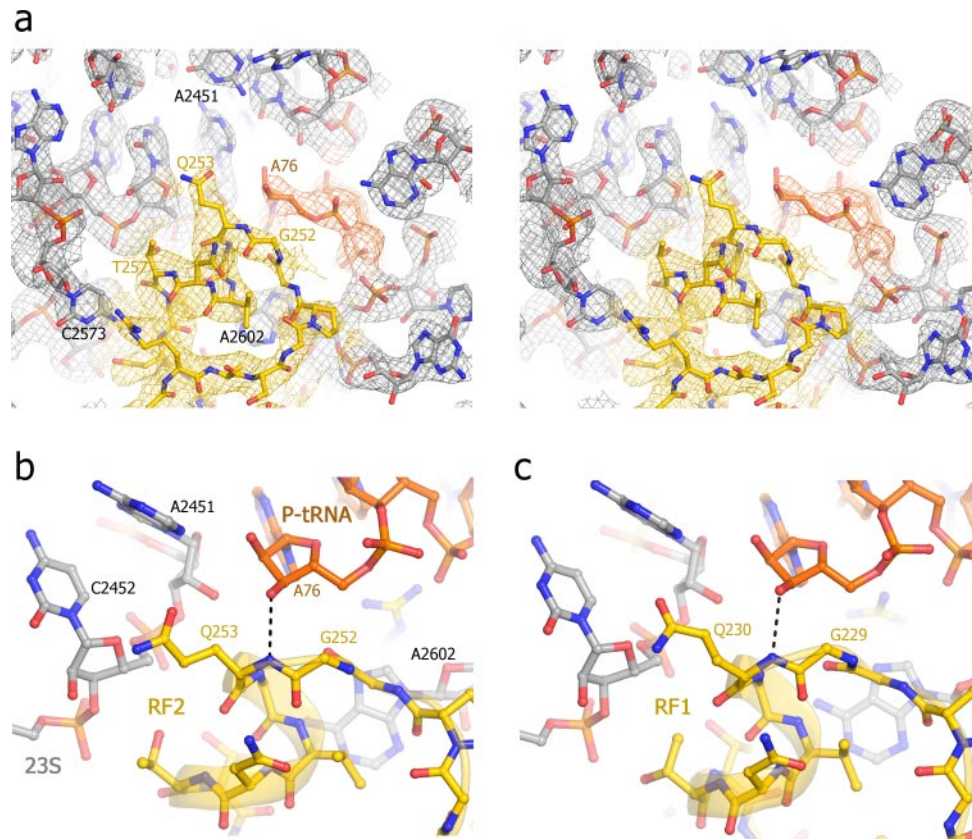


**Fig. S6.** Interactions of the universally conserved GGQ motif of RF2 (this work) and RF1 (1) in the peptidyl transferase center (PTC) of the termination complex. (a) Stereoview of  $\sigma_A$ -weighted  $3F_{\text{obs}}-2F_{\text{calc}}$  electron density map for the PTC in the RF2 complex. Densities for RF2 (yellow), P-tRNA (orange) and 23S rRNA (gray) are contoured at  $1.7\sigma$ . (b) Position of the universally conserved Gln-253 of RF2 in the PTC. (c) Position of the universally conserved Gln-230 of RF1 in the PTC.



**Table S1. Rates of RF1-dependent fMet-tRNA hydrolysis**

Release factor	$k_{\text{obsr}} \text{ s}^{-1}$	
	This work	Shaw and Green, 2007*
RF1 (WT)	>0.03	0.65
Q235A	>0.03	0.18
Q235D	$8.6 \times 10^{-5} \pm 0.8 \times 10^{-5}$	$6.8 \times 10^{-5}$
Q235N	$25 \times 10^{-5} \pm 0.1 \times 10^{-5}$	$8.5 \times 10^{-5}$
Q235P	$1.2 \times 10^{-5} \pm 0.09 \times 10^{-5}$	ND
Ribosomes lacking RF1	$1.6 \times 10^{-5} \pm 0.06 \times 10^{-5}$	$1.2 \times 10^{-5}$

Rates of factor-dependent hydrolysis of fMet-tRNA by mutant *E. coli* RF1 were determined as described in *SI Materials and Methods* and in Shaw JJ, Green R (2007) Two distinct components of release factor function uncovered by nucleophile partitioning analysis. *Mol Cell* 28:458–467. In this work, the rapid reaction rates of wild-type RF1 and the Q235A mutant could not be quantified.

**Table S2. X-ray data collection and refinement statistics**

Data collection	
Space group	$P2_1 2_1 2_1$
Cell dimensions	
<i>a</i>	211.24 Å
<i>b</i>	456.78 Å
<i>c</i>	618.71 Å
$\alpha$	90°
$\beta$	90°
$\gamma$	90°
Resolution, Å	50–3.0 (3.11–3.0)*
$R_{p.i.m.}$ *	0.097 (0.308)
$I/\sigma I$	8.8 (2.4)
Completeness, %	97.9 (89.9)
Redundancy	16.8 (8.4)
Refinement	
Resolution, Å	50–3.0
No. reflections	1,148,216
$R_{work}/R_{free}$	0.280/0.316
No. atoms	301,212
Protein atoms	98,072
RNA atoms	200,748
Ions	2,392
rmsd	
Bond lengths, Å	0.006
Bond angles, °	1.20

The highest-resolution shell is shown in parenthesis.

\* $R_{p.i.m.}$  is the precision-indicating merging *R* factor [Weiss MS (2001) Global indicators of X-ray data quality. *J Appl Crystallogr* 34:130–135].